Using interpolation to insert small-scale inhomogeneities in the acoustic finite difference scheme

Ivan Karpov and Børge Arntsen, Norwegian University of Science and Technology; Espen Birger Raknes, Norwegian University of Science and Technology, Aker BP*

SUMMARY

We propose a way to include small-scale inhomogeneities and sharp boundaries in high-order acoustic finite difference schemes. The method is based on representing the inhomogeneities as secondary sources defined on dense auxiliary grids. Interaction of the secondary sources with the finite difference scheme is performed by interpolation. We observe good agreement of the method's results with precise solutions for simple models in 2D.

INTRODUCTION

The finite difference (FD) method (e.g., Virieux, 1986) is likely the most popular method to numerically solve the problem of seismic wave propagation. Development of high-order FD schemes (Holberg, 1987) has made it possible to define the medium parameters on sparse grids with a few grid points per shortest wavelength, which has significantly eased the memory requirements and shortened the computation time. However, small-scale structures and sharp interfaces are poorly resolved by such grids.

Non-uniform grids allow to have higher spatial resolution in chosen domains. Mikumo et al. (1987) used continuous non-uniform grids to reduce the grid spacing in the vicinity of fault planes. Kessler and Kosloff (1991) employed discontinuous non-uniform grids to include boreholes in the wave field computation. Implementation of such an algorithm is not straightforward, and discretization of a model on a non-uniform grid may be tedious. For stability, the time increment in the methods is defined by the smallest grid spacing, which leads to long run-times.

There are solutions that leave the FD grid spacing untouched and hence do not degrade the memory and time advantages of the high-order FD schemes. However, they are limited to specific problems and geometries. Carcione (1996) uses explicit boundary conditions at the crack location; van Baren et al. (2001) approximate small cracks by secondary sources; Coates and Schoenberg (1995) consider cells containing faults as equivalent homogeneous media; in a similar manner, Muir et al. (1992) treat each grid cell containing an interface as an equivalent homogeneous block. Note that the equivalent media in the last two solutions are anisotropic, which requires solving more complex anisotropic equations.

We suggest a simple solution to include arbitrary small-scale structures in the FD scheme while retaining its sparse grid. We split the medium into two parts: a background medium with large-scale structures specified on a sparse FD grid and a perturbed medium with small-scale inhomogeneities defined on separate auxiliary dense grids. We propagate the wave field in the background medium using FD. At each time-step, we update the field with the perturbed medium's response at the auxiliary points. The wave field is extracted at the auxiliary points and injected back in the FD grid with the help of interpolation. Practically, the small-scale inhomogeneities are represented by a number of secondary sources whose strength at a given time step is defined by the structure's properties and the wave field at the previous step.

In the work, we outline the theory of the method and benchmark it against precise solutions for simple cases. We consider acoustic 2D media, though the technique can be readily extended to 3D elastic case.

THEORY

The system of equations governing the acoustic wave propagation is

$$\begin{aligned} \dot{v}_i &= \frac{1}{\rho}\partial_i p + \frac{1}{\rho} f_i \\ \dot{p} &= \kappa \partial_i v_i + \dot{s} \end{aligned} \quad , \tag{1}$$

where ρ is the density, κ is the bulk modulus, v_i is ith component of the displacement velocity, p is the pressure, f_i and s are the displacement velocity source and the pressure source, respectively. Einstein's summation convention for the repeated indexes is implied. The dot means the time derivative. Let us omit the source terms. Suppose the actual medium can be split into a background medium with parameters κ^0, ρ^0 and a perturbed medium κ^1, ρ^1

$$\begin{aligned} \rho &= \rho^0 + \rho^1 \\ \kappa &= \kappa^0 + \kappa^1 \end{aligned} \tag{2}$$

By substituting (2) into (1) and rearranging the terms, we get

$$\begin{aligned} \dot{v}_i &= \frac{1}{\rho^0}\partial_i p - \frac{\rho^1}{\rho^0}\dot{v}_i \\ \dot{p} &= \kappa^0 \partial_i v_i + \kappa^1 \partial_i v_i \end{aligned} \tag{3}$$

System (3) describes the full wave field propagation in the background medium, where the last terms on the right-hand side can be viewed as secondary sources introducing the wave generated by the perturbation into the model. Any FD algorithm can be easily modified to handle (3). The background parameters κ^0, ρ^0 define

10.1190/segam2018-2997751.1

the FD grid properties. Notice that (2) do not include any restrictions on the perturbation parameters.

We define perturbations κ^1, ρ^1 on a dense auxiliary grid disconnected from the FD grid. At each time step in FD, we compute $\dot{v}_i$ and $\partial_i v_i$ at the auxiliary grid points, scale them by $-\rho^1/\rho^0$ and κ^1, respectively, scale the results by the auxiliary cell volume in accordance with the rectangle integration rule, and re-inject the fields in the same auxiliary points.

Normally, the points do not coincide with the FD grid nodes. We use Hicks' interpolation (Hicks, 2002) to link the grids. The method is based on Kaiser-windowed sinc-functions. It provides accurate results when the medium is homogeneous within the interpolation window, and when the source point is sufficiently distant from the receiver point.

RESULT

First, we consider a simple problem of the acoustic wave scattering from a circular inhomogeneity in 2D. We compute the scattered field using the algorithm described before as well as the pure FD solution with a few FD nodes specifying the inhomogeneity. We benchmark the results against an analytical solution (Bowman et al., 1969). In order to extract the scattered field, we compute the full wave field using (3) and subtract the background field computed in the same background model without the secondary sources.

Fig. 1 depicts the acquisition geometry. The pressure wave is excited by a point source offset at 400 m from a circular inhomogeneity's axis. The scattered pressure wave is recorded in a number of points evenly distributed on a semicircle with radius 200 m around the center of the structure. The circular inhomogeneity has radius of 40 m and takes on 50% perturbations in the bulk modulus and the density, i.e.

$$\begin{aligned} \delta\rho &= \frac{\rho^1}{\rho^0}\cdot 100\% = 50\% \\ \delta\kappa &= \frac{\kappa^1}{\kappa^0}\cdot 100\% = 50\% \end{aligned}, \qquad (4)$$

where the background medium is water with κ^0=2.25 $\cdot$ 10^9 Pa and ρ^0=1000 kg/m^3.

We use the second order in time and eighth order in space staggered grid FD scheme (Virieux, 1986; Holberg, 1987). The grid spacing in both spatial dimensions is 20 m. The source wavelet is the Ricker pulse with central frequency 10 Hz. The time step is equal to 1 ms. We interpolate the wave fields at source, receiver and auxiliary grid locations using Hicks' interpolation with a window of half-width equal to 4 nodes. Relation of the circle to the FD grid is illustrated in Fig. 2. The black and blue dots are the pressure and displacement velocity FD nodes. The inhomogeneity (pink circle) is defined on a 15×15 nodes auxiliary grid (red points).

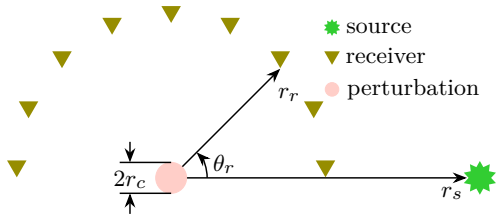

Figure 1: Acquisition configuration for the scattering from a circular inhomogeneity. Circular inhomogeneity with radius r_c=40 m (pink), point pressure source (green) is offset at r_s=400 m from the inhomogeneity's axis, pressure receivers (olive) are evenly distributed on a semicircle with r_r=200 m around the perturbation.

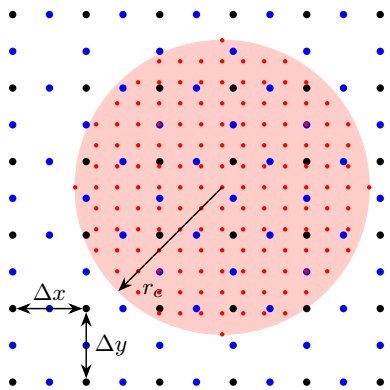

Figure 2: Circular inhomogeneity with radius r_c=40 m (pink) is specified by an auxiliary grid (red). Pressure (black) and displacement velocity (blue) FD nodes have spacing Δx=Δy=20 m.

Fig. 3 shows the normalized scattered pressure field. The proposed secondary source technique (red dashed line) provides close fit to the exact analytical solution (blue solid) almost everywhere. Observe that although the wave field in the FD scheme is propagated in the background medium (3), the continuous feedback from the inhomogeneity ensures the correct phase shift. The pure FD solution where the inhomogeneity is described by a few grid nodes is off both in amplitude and phase (yellow dotted).

In the second experiment, we consider a non-isometric body – a thin horizontal layer in a homogeneous medium. Fig. 4 outlines the problem's geometry. The thickness of the layer is 80 m. It takes on 50% perturbations both in density and bulk modulus. The FD grid step in both spatial dimensions is 20 m, so there are only a few rows of the FD grid points to represent the structure. In turn, the auxiliary grid has 2.5 m vertical step and 20 m horizontal step. In FD and the secondary source approach, the model is long enough to avoid the edge effects and to mimic the infinite span of the layer. All other parameters are the same as in the previous experiment.

10.1190/segam2018-2997751.1

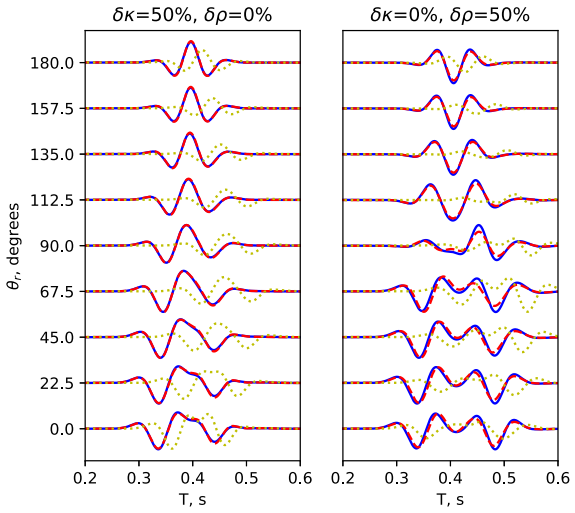

Figure 3: The normalized pressure field scattered from the small circular inhomogeneity with r_c=40 m. Comparison of results of the secondary source technique (red dashed), the pure FD solution with a few grid nodes representing the structure (yellow dotted) and the analytical solution (blue solid). 50% perturbation in bulk modulus (left) and density (right) is applied.

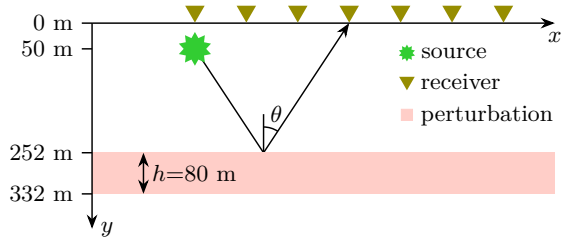

Figure 4: Acquisition configuration for the scattering on a thin horizontal layer. The pressure wave is emitted by a point source (green), reflected from the layer (pink) and recorded in a linear receiver array (olive) at different reflection angles $\theta \in [0°, 60°]$.

We compute the reflected wave field using the secondary source approach and the pure FD scheme, and benchmark them against a semi-analytical solution obtained with the global matrix approach (Schmidt and Tango, 1986). Fig. 5 shows the normalized reflected field for different reflection angles. The direct wave is neglected. The pure FD solution (yellow dotted) is close to the semi-analytical one in case the bulk modulus is perturbed (Fig. 5, left), though there is a noticeable phase error. In the case of density perturbation (Fig. 5, right), the pure FD solution is much less accurate due to dispersion (the wavelength in the layer is small). The secondary source solution is unconditionally better in both cases, even though the FD parameters are exactly the same.

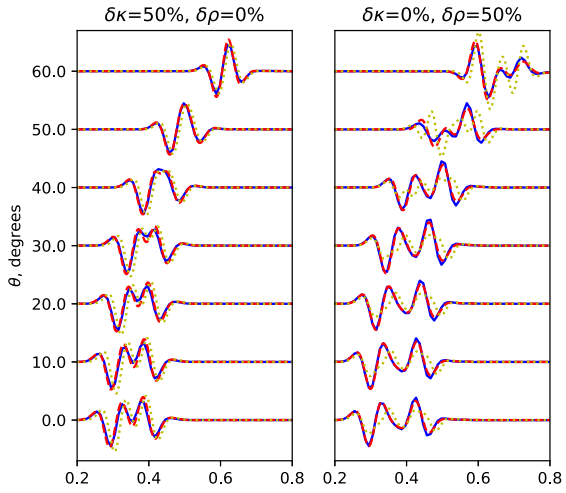

Figure 5: The normalized pressure field reflected by the thin layer with h=80 m. Comparison of results of the secondary source technique (red dashed), the pure FD solution with a few grid rows representing the structure (yellow dotted) and the semi-analytical solution (blue solid). 50% perturbation in bulk modulus (left) and density (right) is applied.

DISCUSSION

The stability criterion for the acoustic FD scheme we use is (Holberg, 1987)

$$\Delta t < \frac{\sqrt{2}h}{\pi c} \quad , \tag{5}$$

where h=Δx=Δy, c is the wave velocity, and Δt is the time increment. For the background medium we used in the first experiment (κ=$2.25 \cdot 10^9$ Pa, ρ=1000 kg/m^3, Δx=Δy=20 m) the time increment should be less than 6 ms. If we derive Δt for the perturbation with the highest velocity in the first experiment and the auxiliary grid spacing (κ=$3.375 \cdot 10^9$ Pa, ρ=1000 kg/m^3, Δx=Δy=5.71 m) it should be less than 1.4 ms. In the computations, the time step value was 1 ms, which we expected would guarantee stability of the method. However, at late times the secondary source representation blows out (Fig. 6). The method's stability is yet to be analyzed.

The interpolation method we used does not ensures correct results if there are inhomogeneities in the background medium within the interpolation window (Hicks, 2002). Generally, small-scale structures are not restricted to homogeneous domains, and one potentially may want to simulate their presence in the vicinity of a large-scale boundary. The behavior of the algorithm should be studied for this case.

The idea to represent inhomogeneities as secondary sources is not limited to FD and can be implemented in other

10.1190/segam2018-2997751.1

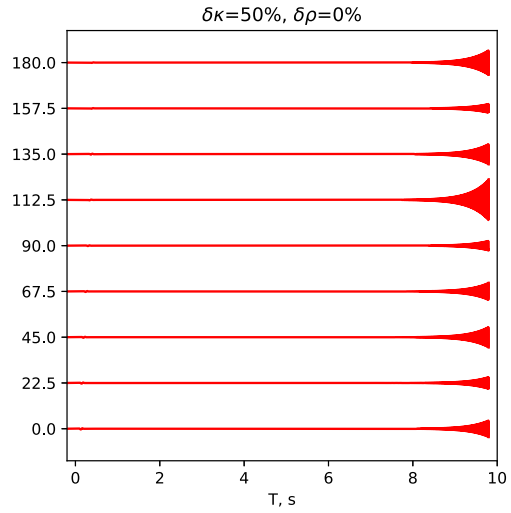

Figure 6: The pressure field scattered from the small circular inhomogeneity with r_c=40 m and 50% perturbation in bulk modulus obtained with the secondary source technique. Observe the instability at late times.

numerical methods. The spectral element method (Komatitsch and Tromp, 1999) is the best candidate since it has its inherent interpolation within each element, and the problem of having an interface in the vicinity of the small inhomogeneity will not arise there.

The application of the idea to elasticity is as follows. The system of equations governing the elastic wave propagation is

$$\begin{aligned} \dot{v}_i &= \frac{1}{\rho}\partial_j \sigma_{ij} + \frac{1}{\rho} f_i \\ \dot{\sigma}_{ij} &= \delta_{ij}\lambda \dot{\varepsilon}_{kk} + 2\mu \dot{\varepsilon}_{ij} + \dot{s}_{ij} \quad , \\ \dot{\varepsilon}_{ij} &= \frac{1}{2}\left(\partial_j v_i + \partial_i v_j\right) \end{aligned} \tag{6}$$

where v_i is the ith component of the displacement velocity vector, σ_{ij} is the stress tensor, ε_{ij} is the strain tensor, δ_{ij} is the Kronecker delta, λ and μ are the Lamé parameters, ρ is the density, f_i and s_{ij} are the source terms. Dot means the time derivative, and Einstein's summation convention is used. If we split the medium parameters into the large-scale ρ^0, λ^0, μ^0 and small-scale ρ^1, λ^1, μ^1 parts

$$\begin{aligned} \rho &= \rho^0 + \rho^1 \\ \lambda &= \lambda^0 + \lambda^1 \quad , \\ \mu &= \mu^0 + \mu^1 \end{aligned} \tag{7}$$

substitute them in (6) and rearrange the terms, we get (the source terms are omitted)

$$\begin{aligned} \dot{v}_i &= \frac{1}{\rho^0}\partial_j \sigma_{ij} - \frac{\rho^1}{\rho^0}\dot{v}_i \\ \dot{\sigma}_{ij} &= \delta_{ij}\lambda^0 \dot{\varepsilon}_{kk} + 2\mu^0 \dot{\varepsilon}_{ij} + \delta_{ij}\lambda^1 \dot{\varepsilon}_{kk} + 2\mu^1 \dot{\varepsilon}_{ij} \end{aligned} \tag{8}$$

Again, the terms with the small-scale medium parameters can be treated as secondary sources, can be defined on dense auxiliary grids and inserted in FD with the aid of interpolation.

CONCLUSIONS

A simple way to include small-scale inhomogeneities in FD is presented. We define the structures as secondary sources on dense auxiliary grids and sew them into the finite difference scheme with interpolation. The auxiliary grid should not necessarily be rectangular, but can be irregular, curvilinear, etc., as long as the integration weights for each secondary source are correctly estimated. Implementation of the algorithm does not require much effort, any existing FD solver for the wave equation can be easily modified to use the idea. We tested the algorithm in two simple 2D acoustic cases and observed good fit with the known exact solutions.

The method has possibilities for improvement: its stability should be analyzed, different interpolation strategies need to be attempted. However, the principal possibility to use it for small-scale structures in FD is shown.

ACKNOWLEDGMENTS

This project has received funding from the European Union's Horizon 2020 research and innovation programme under the Marie Sklodowska-Curie grant agreement No 641943. The authors would like to thank NTNU and Aker BP ASA for making the code available through the Codeshare project.

REFERENCES

Bowman, J. J., T. B. A. Senior, and P. L. E. Uslenghi, eds., 1969, Electromagnetic and acoustic scattering by simple shapes: North-Holland Publishing Company.

Carcione, J. M., 1996, Scattering of elastic waves by single anelastic cracks and fractures: 66th Annual International Meeting, SEG, Expanded Abstracts, 654–657, https://doi.org/10.1190/1.1826732.

Coates, R. T., and M. Schoenberg, 1995, Finite-difference modeling of faults and fractures: Geophysics, **60**, 1514–1526, https://doi.org/10.1190/1.1443884.

Hicks, G. J., 2002, Arbitrary source and receiver positioning in finite-difference schemes using Kaiser windowed sinc functions: Geophysics, **67**, 156–165, https://doi.org/10.1190/1.1451454.

Holberg, O., 1987, Computational aspects of the choice of operator and sampling interval for numerical differentiation in large-scale simulation of wave phenomena: Geophysical Prospecting, **35**, 629–655, https://doi.org/10.1111/j.1365-2478.1987.tb00841.x.

Kessler, D., and D. Koslo, 1991, Elastic wave propagation using cylindrical coordinates: Geophysics, **56**, 2080–2089, https://doi.org/10.1190/1.1443020.

Komatitsch, D., and J. Tromp, 1999, Introduction to the spectral element method for three-dimensional seismic wave propagation: Geophysical Journal International, **139**, 806–822, https://doi.org/10.1046/j.1365-246x.1999.00967.x.

Mikumo, T., K. Hirahara, and T. Miyatake, 1987, Dynamical fault rupture processes in heterogeneous media: Tectonophysics, **144**, 19–36, https://doi.org/10.1016/0040-1951(87)90006-0.

Muir, F., J. Dellinger, J. Etgen, and D. Nichols, 1992, Modeling elastic fields across irregular boundaries: Geophysics, **57**, 1189–1193, https://doi.org/10.1190/1.1443332.

Schmidt, H., and G. Tango, 1986, Efficient global matrix approach to the computation of synthetic seismograms: Geophysical Journal International, **84**, 331–359, https://doi.org/10.1111/j.1365-246X.1986.tb04359.x.

van Baren, G. B., W. A. Mulder, and G. C. Herman, 2001, Finite-difference modeling of scalar-wave propagation in cracked media: Geophysics, **66**, 267–276, https://doi.org/10.1190/1.1444905.

Virieux, J., 1986, P-SV wave propagation in heterogeneous media: Velocity-stress finite-difference method: Geophysics, **51**, 889–901, https://doi.org/10.1190/1.1442147.